GSA Data Repository Item 2018115

Haroldson, E.L., Beard, B.L., Satkoski, A.M., Brown, P.E., and Johnson, C.M., 2018, Gold remobilization associated with Mississippi Valley–type fluids: A Pb isotope perspective: GSA Bulletin, https://doi.org/10.1130/B31901.1.

# DATA REPOSITORY

## FURTHER METHODOLOGY OF LA-ICP-MS PB ISOTOPE ANALYSIS

Details of the methods used for Pb isotope analysis by femto second laser ablation (fsLA) are reported below. Helium was used as a carrier gas to transport LA-generated particles out of the HelEx cell to the plasma. Just prior to the ICP torch, Ar from a Cetac Aridus II was added to the LA stream by connecting the sample-out tubing from the Aridus to a glass tee connected to the torch. The aerosol from the laser ablation cell was connected to the part of the tee that was in line with the torch and the sample out from the Aridus was connected to the part of the tee normal to the torch. The flow rate of He added to the arm of the HelEx cell was 0.25 L per minute and the flow rate to the large part of the cell was 0.45 L per minute. The Aridus was operated with a nebulizer pressure of 40 psi, which supplied gas to a Savillex self-aspirating concentric nebulizer that had an uptake rate of ~125μl/minute. The sweep gas of the Aridus was set to 5.4 L per minute. These tuning conditions were established by maximizing the Pb ion signal during ablation of NIST glass SRM610 with the pulse energy of the laser increased to 10 μJ. A higher pulse energy was used because at the low fluence used for the Pb isotope analyses of Pb sulfides and tellurides, the NIST glasses are poorly ablated. Use of the Aridus allowed us to add Tl to the LA-generated particles, which was used to correct for instrumental mass bias. Under these He and Ar gas flow conditions, Pb and Tl solutions aspirated into the mass spectrometer from the Aridus produced an instrument sensitivity of ~750 V per ppm for both Pb and Tl. For comparison, the sensitivity of the instrument when it is tuned for maximum sensitivity with only the Aridus connected to the torch is 1250 V/ppm. The lower sensitivity for LA setup is caused because of the He addition and because the Aridus sweep gas is a lower value as compared to when the instrument is setup for only introduction of material from the Aridus.

Laser ablation Pb isotope ratio analyses were collected using the time-resolved analysis feature of the Nu Plasma software and are based on 100 seconds of data collection while firing the laser for 125 shots at a repetition rate of 4.03 Hz. During the ablations a 10 ppb solution of Tl made from NIST SRM-997 was aspirated into the Aridus. All measurements were performed using Faraday collectors fitted with $1 \times 10^{11}$ ohm resistors. Ion signals were corrected for background by subtracting on-peak zeros that were measured for 60 seconds at the beginning of an analysis session in which 2% $HNO_3$ was aspirated into the Aridus and the laser was not fired. All Pb isotope ratios were corrected for mass bias using an exponential mass-bias factor based on the measured $^{205}Tl/^{203}Tl$ ratio of Tl that was aspirated into the Aridus and applying that beta value directly to the measured Pb isotope ratios. Isobars of $^{204}Hg$ at mass $^{204}Pb$ were monitored at mass $^{202}Hg$ and $^{201}Hg$ and were found to be 0 after on-peak-zero subtraction and thus no Hg correction was applied. The mass-bias-corrected ratios were then normalized to the average Pb isotope composition of NIST SRM-981 that was analyzed at the beginning and end of every analysis session, assuming Pb isotope ratios for SRM-981 to be equal to those measured by Galer and Abouchami (1998).

To test accuracy of this LA method, a natural mineral standard was developed. The standard used was pyrite from the Rio Tinto mine (Spain) collected from near the abandoned T16 train tunnel. The Rio Tinto pyrite is essentially devoid of Pb (the Pb ion signal during ablation of pyrite was ~$5 \times 10^3$ counts per second as measured using ion counters), except for small micron-sized grains of galena that occur as inclusions in pyrite or between pyrite grains (Figure DR-2). To determine the homogeneity of Pb from galena in these pyrite grains, 22 conventional solution analyses of pyrite that weighed between 0.2 and 2 mg were performed. The measured Pb concentration of these different pyrite dissolutions was highly variable (50,000–500 ppm Pb), but the Pb isotope ratios were homogenous. The variable Pb concentrations are interpreted to be a result of the inhomogeneous distribution of galena in the pyrite but the homogenous Pb isotope ratios indicate that these galena crystals all have the same Pb isotope composition. Laser ablation analyses of galena inclusions identified by SEM were interspersed during the LA analysis of the Reef samples. Total Pb ion signals (the sum of $^{204}$Pb, $^{206}$Pb, $^{207}$Pb and $^{208}$Pb voltages) for 21 analyses of this pyrite standard ranged from 66 to 1.4 total Pb volts and the measured Pb isotope ratios match those of the conventional solutions analyses (Table 1). The range in Pb ion signals reflects the relative size of the galena crystals and, because of the Gaussian beam profile of a fs-laser, the position of the laser spot with respect to the measured galena crystal. The reproducibility of these Rio Tinto pyrite/galena standards is 0.12% per atomic mass unit and we believe that the external precision of the Pb isotope ratios of the Reef samples is the same because the Reef samples had the same range in total ion signals as that measured for the Rio Tinto pyrite/galena standard. We highlight that because the area of ablation was larger than the phase of interest and the amount of that phase being ablated at any particular time is variable, the total Pb ion intensity was variable for any giving analysis and thus it is not possible to use ion intensity to infer Pb concentration in the Pb-rich phase.

## REFERENCES CITED

Galer S.J.G., Abouchami W., 1998, Practical application of lead triple spiking for correction of instrumental mass discrimination, Mineralogical Magazine, vol 62(A), p.491–492, doi: DOI: 10.1180/minmag.1998.62A.1.260

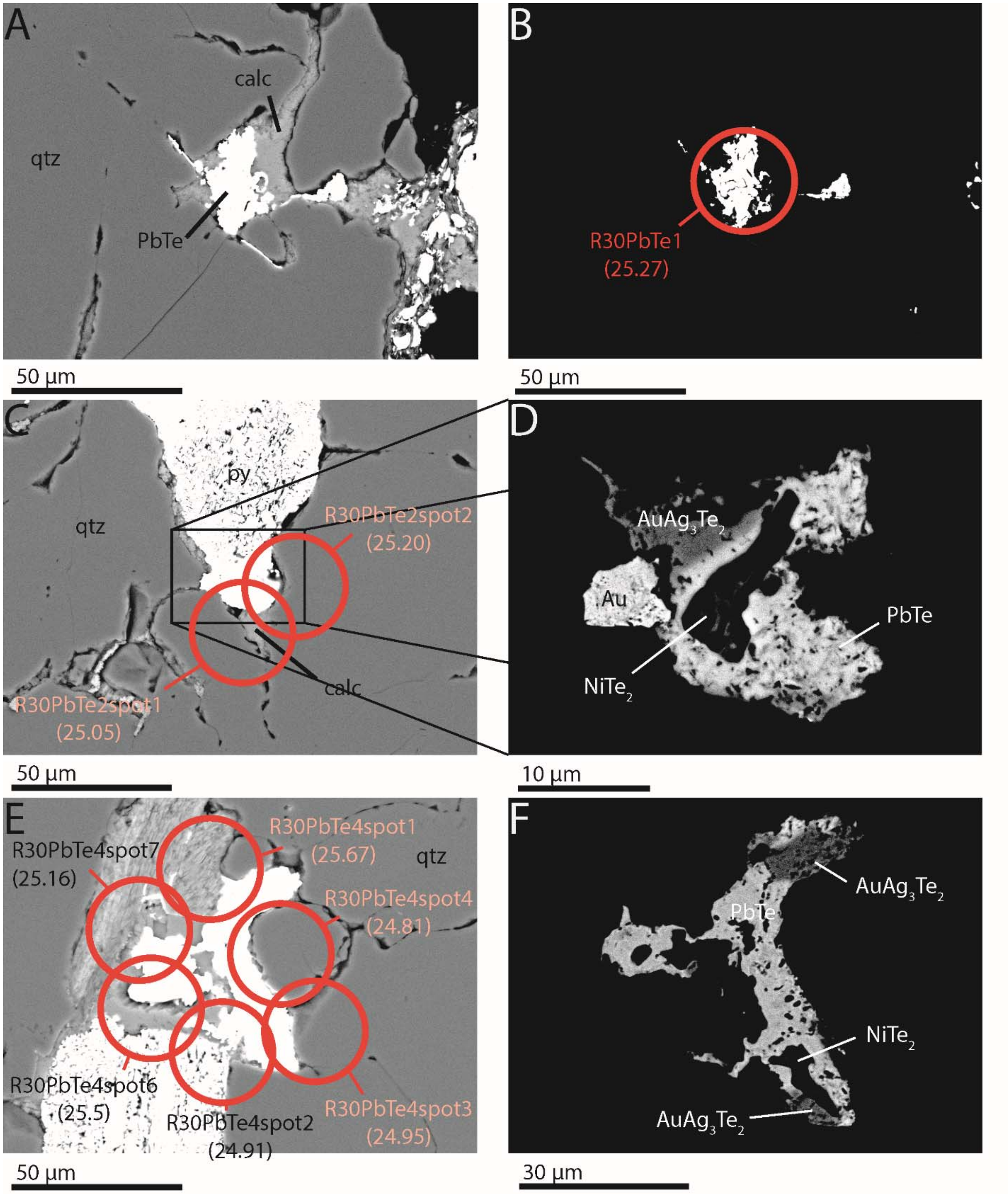
A
calc
qtz
PbTe
50 µm
B
R30PbTe1
(25.27)
50 µm
C
py
qtz
R30PbTe2spot2
(25.20)
R30PbTe2spot1
(25.05)
calc
50 µm
D
AuAg3Te2
Au
PbTe
NiTe2
10 µm
E
R30PbTe4spot1
(25.67)
qtz
R30PbTe4spot7
(25.16)
R30PbTe4spot4
(24.81)
R30PbTe4spot6
(25.5)
R30PbTe4spot2
(24.91)
R30PbTe4spot3
(24.95)
50 µm
F
AuAg3Te2
PbTe
NiTe2
AuAg3Te2
30 µm

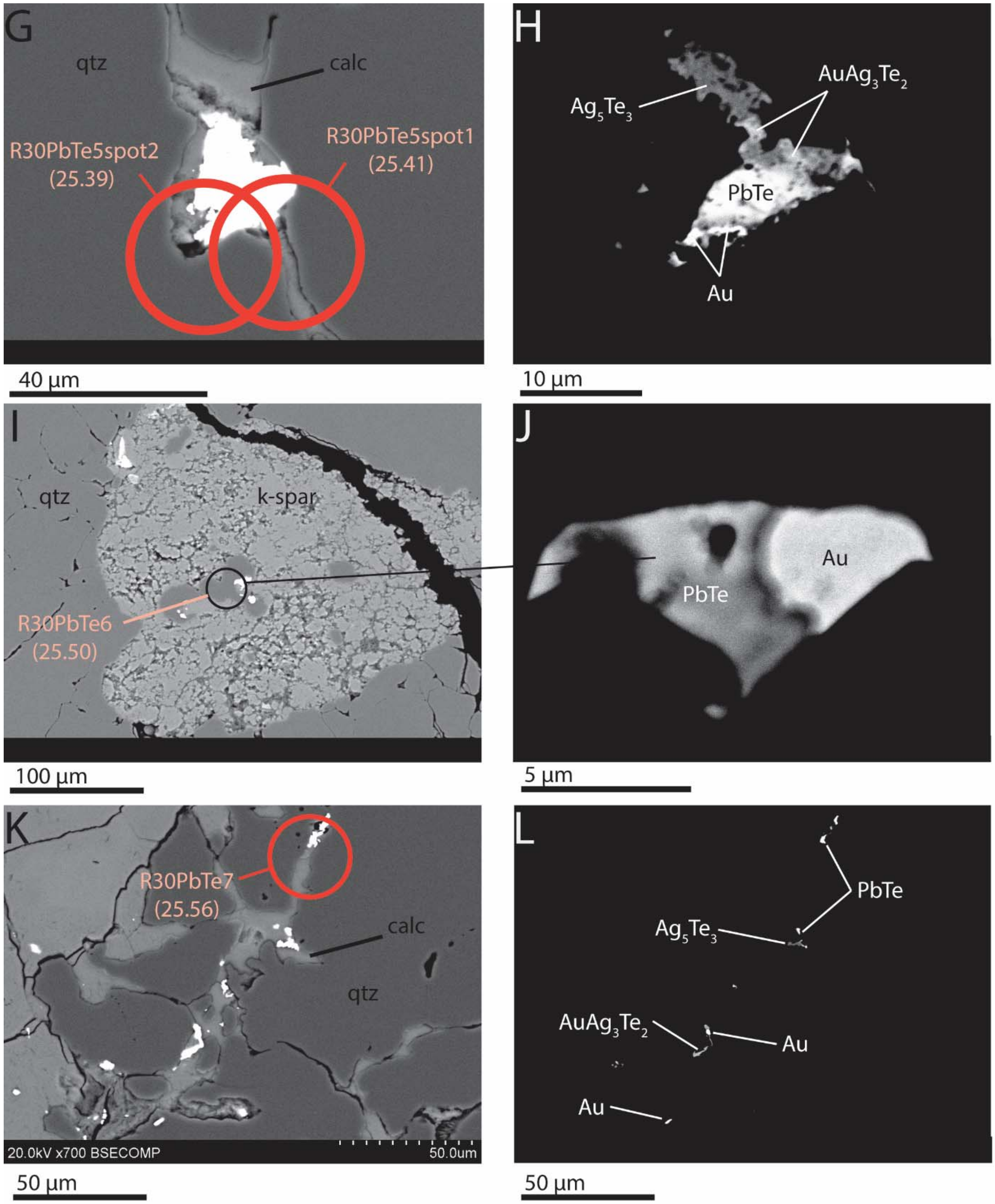
G
qtz
calc
R30PbTe5spot2
(25.39)
R30PbTe5spot1
(25.41)
40 µm
H
$Ag_5Te_3$
$AuAg_3Te_2$
PbTe
Au
10 µm
I
qtz
k-spar
R30PbTe6
(25.50)
100 µm
J
PbTe
Au
5 µm
K
R30PbTe7
(25.56)
calc
qtz
20.0kV x700 BSECOMP
50.0um
50 µm
L
PbTe
$Ag_5Te_3$
$AuAg_3Te_2$
Au
Au
50 µm

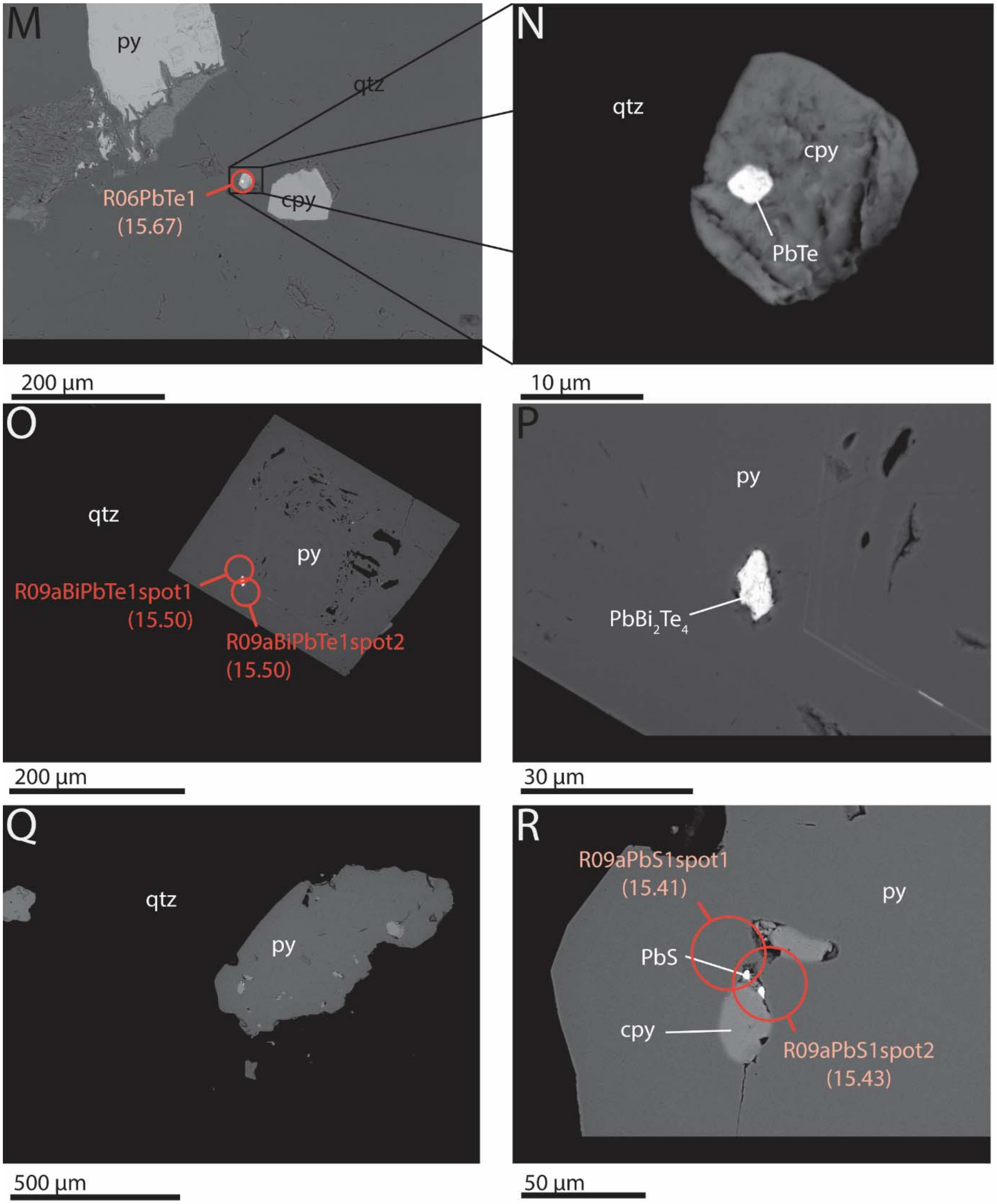
M
py
qtz
R06PbTe1
(15.67)
cpy
200 µm
N
qtz
cpy
PbTe
10 µm
O
qtz
py
R09aBiPbTe1spot1
(15.50)
R09aBiPbTe1spot2
(15.50)
200 µm
P
py
PbBi2Te4
30 µm
Q
qtz
py
500 µm
R
R09aPbS1spot1
(15.41)
py
PbS
cpy
R09aPbS1spot2
(15.43)
50 µm

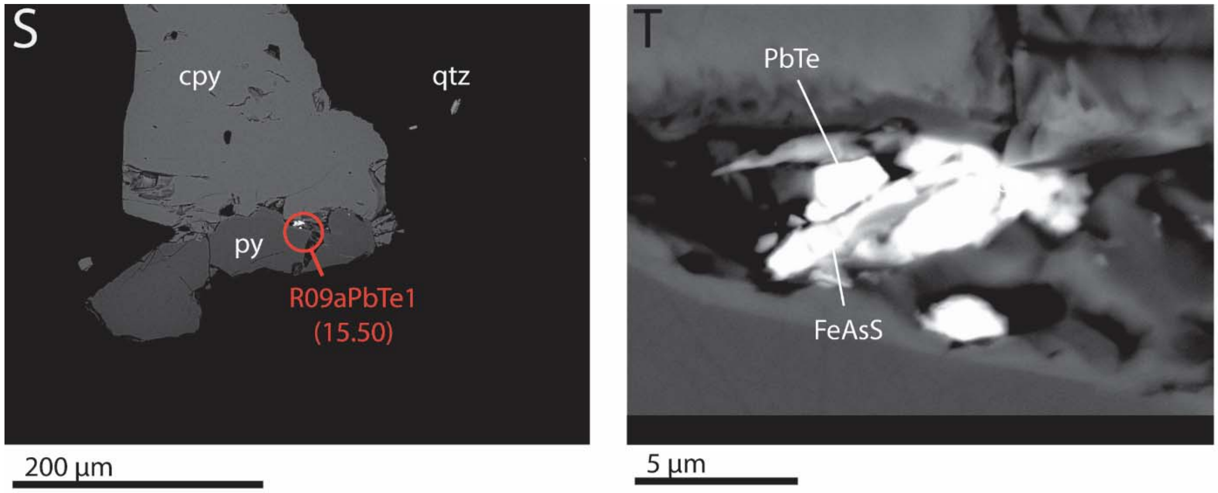


**Figure DR-1**. (A) – (T) Backscattered electron images of Pb-rich phases analyzed by femtosecond laser ablation and MC-ICP-MS. Left column shows textural relationship with surrounding host, right column images are magnified and have a similar or lowered brightness setting to show intergrowth of various phases. Red circles show location of analyses and each is labeled with the sample number from Table 2 (measured $^{206}Pb/^{204}Pb$ isotope ratio is in parentheses).

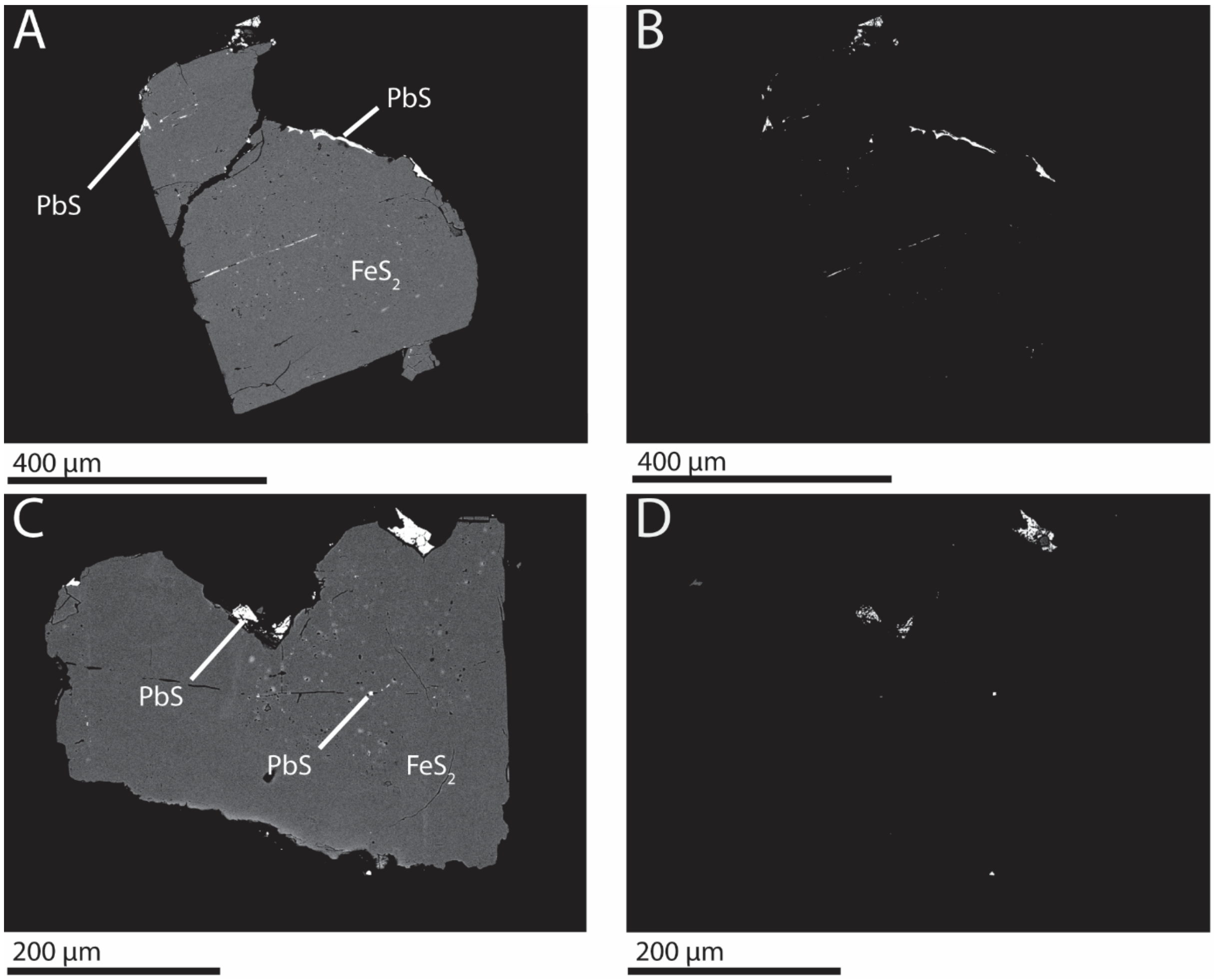


**Figure DR-2**. Backscattered electron images of Rio Tinto standard grains mounted in epoxy. Left column shows total grain, right column images have a lowered brightness setting to show the galena on grain boundaries and along fractures.

**TABLE DR-1.** MEASURED PB ISOTOPE COMPOSITIONS OF RIO TINTO PYRITE STANDARD

| Sample ID | Total Pb V | $^{206}Pb/^{204}Pb$ | $^{207}Pb/^{204}Pb$ | $^{208}Pb/^{204}Pb$ | $^{207}Pb/^{206}Pb$ | $^{208}Pb/^{206}Pb$ |
|---|---|---|---|---|---|---|
| *Solution analyses of 0.2–3 mg sized dissolutions of the Rio Tinto Pyrite* | | | | | | |
| Rio Tinto B | | 18.199 | 15.635 | 38.247 | 0.8591 | 2.1016 |
| Rio Tinto C | | 18.199 | 15.634 | 38.248 | 0.8591 | 2.1017 |
| Rio Tinto D | | 18.193 | 15.633 | 38.239 | 0.8593 | 2.1019 |
| 5P-187 | | 18.198 | 15.636 | 38.249 | 0.8592 | 2.1018 |
| 5P-187 | | 18.198 | 15.636 | 38.248 | 0.8592 | 2.1017 |
| 5P-188 | | 18.199 | 15.635 | 38.246 | 0.8591 | 2.1016 |
| 5P-188 | | 18.199 | 15.635 | 38.246 | 0.8591 | 2.1015 |
| 5P-189 | | 18.199 | 15.636 | 38.247 | 0.8592 | 2.1017 |
| 5P-189 | | 18.199 | 15.637 | 38.249 | 0.8592 | 2.1017 |
| 5P-190 | | 18.200 | 15.636 | 38.249 | 0.8591 | 2.1016 |
| 5P-190 | | 18.198 | 15.635 | 38.248 | 0.8591 | 2.1017 |
| 5P-191 | | 18.197 | 15.637 | 38.248 | 0.8593 | 2.1019 |
| 5P-191 | | 18.194 | 15.634 | 38.241 | 0.8593 | 2.1018 |
| 5P-192 | | 18.192 | 15.633 | 38.235 | 0.8593 | 2.1018 |
| 5P-192 | | 18.190 | 15.631 | 38.227 | 0.8593 | 2.1015 |
| 5P-193 | | 18.191 | 15.633 | 38.234 | 0.8593 | 2.1018 |
| 5P-193 | | 18.191 | 15.634 | 38.235 | 0.8594 | 2.1018 |
| 5P-194 | | 18.196 | 15.637 | 38.250 | 0.8593 | 2.1021 |
| 5P-195 | | 18.199 | 15.636 | 38.251 | 0.8592 | 2.1019 |
| 5P-195 | | 18.197 | 15.635 | 38.247 | 0.8592 | 2.1018 |
| 5P-196 | | 18.194 | 15.636 | 38.242 | 0.8594 | 2.1019 |
| 5P-196 | | 18.196 | 15.637 | 38.247 | 0.8594 | 2.1020 |
| **Mean** | | **18.196** | **15.635** | **38.244** | **0.8592** | **2.1018** |
| **2-SD** | | **0.006** | **0.003** | **0.013** | **0.0002** | **0.0003** |
| *Laser ablation analyses of galena nuggets in the Rio Tinto Pyrite* | | | | | | |
| run 4A | 24.23 | 18.19 | 15.64 | 38.23 | 0.859 | 2.101 |
| run 4B | 16.88 | 18.21 | 15.65 | 38.24 | 0.859 | 2.100 |
| run 4C | 2.88 | 18.21 | 15.65 | 38.23 | 0.859 | 2.100 |
| run 4D | 10.12 | 18.23 | 15.66 | 38.25 | 0.859 | 2.099 |
| run 4E | 9.81 | 18.18 | 15.63 | 38.22 | 0.859 | 2.102 |
| Rs01_RTcg2_spot1 | 66.47 | 18.18 | 15.62 | 38.21 | 0.859 | 2.101 |
| Rs01_RTcg2_spot2 | 33.40 | 18.18 | 15.62 | 38.21 | 0.859 | 2.102 |
| R30_RTCG2_spot1 | 4.78 | 18.23 | 15.67 | 38.22 | 0.860 | 2.096 |
| R30_RTCG2_spot2 | 15.93 | 18.18 | 15.63 | 38.18 | 0.859 | 2.099 |
| R30_RTCG2_spot3 | 1.96 | 18.18 | 15.63 | 38.15 | 0.859 | 2.098 |
| R30_RTCG2_spot4 | 3.18 | 18.23 | 15.67 | 38.19 | 0.860 | 2.095 |
| R30_RTCG2_spot5 | 14.25 | 18.20 | 15.65 | 38.20 | 0.860 | 2.100 |
| R30_RTcg5_Tl_only_spot2 | 10.73 | 18.19 | 15.63 | 38.21 | 0.859 | 2.101 |
| R30_RTcg5_Tl_only_spot3 | 2.52 | 18.16 | 15.61 | 38.15 | 0.859 | 2.101 |
| R30_RTcg5_Tl_only_spot4 | 1.97 | 18.15 | 15.59 | 38.14 | 0.859 | 2.099 |
| R30_RTcg5_Tl_only_spot5 | 1.09 | 18.14 | 15.59 | 38.10 | 0.859 | 2.100 |
| Rs02_RT04_01 | 7.03 | 18.26 | 15.69 | 38.27 | 0.859 | 2.097 |
| Rs02_RT07_01 | 17.97 | 18.19 | 15.62 | 38.21 | 0.859 | 2.100 |
| Rs02_RT10_01 | 1.39 | 18.25 | 15.67 | 38.29 | 0.859 | 2.099 |
| Rs02_RT10_02 | 2.29 | 18.26 | 15.68 | 38.29 | 0.859 | 2.098 |
| Rs02_RT10_03 | 6.51 | 18.23 | 15.66 | 38.26 | 0.859 | 2.099 |
| **Mean** | | **18.20** | **15.64** | **38.21** | **0.8593** | **2.099** |
| **2-SD** | | **0.07** | **0.06** | **0.10** | **0.0005** | **0.004** |